Collisional disruption experiments of porous targets

Nakamura, Akiko M.
Hiraoka, Kensuke
Yamashita, Yasuyuki
Machii, Nagisa

(Citation)
Planetary and Space Science,57(2):111-118

(Issue Date)
2009-02

(Resource Type)
journal article

(Version)
Accepted Manuscript

(URL)
https://hdl.handle.net/20.500.14094/90000977

Collisional disruption experiments of porous targets

Akiko M. Nakamura[1], Kensuke Hiraoka[2], Yasuyuki Yamashita[1], and Nagisa Machii[1]

[1] Graduate School of Science, Kobe University, 1-1 Rokkodai-cho, Nada-ku, Kobe, 657-8501, Japan.

[2] Graduate School of Science and Technology, Kobe University

Submitted to Planetary and Space Science

5 figures

Corresponding author:

Akiko M. Nakamura, Dr.

Graduate School of Science, Kobe University, 1-1 Rokkoda-cho, Nada-ku,

Kobe 657-8501, Japan.

E-mail: amnakamu@kobe-u.ac.jp, Tel&Fax: +81-78-803-6483

Abstract

More and more small bodies are found to be porous. Laboratory impact experiments of various porous materials have been performed and increased our understanding of the impact process of porous bodies. In this review, we classify porous targets according to the internal structure, describe the physical properties that characterize these materials, and summarize some results of impact strength and the general tendency upon impact condition and material properties. The material property presented here includes a relation between applied load and distension although measured in static condition. Further investigation is required to clarify the role of crack growth and compaction in the time evolution of physical properties of porous materials upon impact. Laboratory experiments with detailed material properties will be useful as a database that can serve as a reference for numerical modeling and theoretical scaling considerations.

.

1. Introduction

Recent spacecraft explorations and ground-based observations of asteroids have revealed that more and more bodies are porous. The meteorite materials that are thought to be representative of some of asteroid materials are also shown to include microscopic porosity between grain boundaries (e.g., Britt et al. 2002, Fujiwara et al. 2006). The outcomes of collisional disruption of porous bodies have become even more of great significance for studying the origins and collisional evolution of small bodies, although the detailed internal structure, e.g., the size of the pores nor whether or not the body is bounded only by self-gravity, has not fully revealed yet.

Laboratory studies on the impact process of small bodies have provided quantitative data and insights into many aspects of centimeter-scale impact processes, especially for brittle solid materials (Holsapple et al. 2002). The application of the results of laboratory impact experiments to the impact process of small bodies is encouraged by striking similarity in shapes and structure between boulders on asteroid 25143 Itokawa and laboratory rock impact fragments despite differences of orders of magnitude in scale (Nakamura et al. 2008).

Impact strength, Q^*, is a widely used measure of the resistance of small body against collisional disruption in such laboratory studies and numerical modeling. It is

the threshold value of energy density (that is the kinetic energy of the colliding bodies per the mass of the larger body, Q) for catastrophic disruption that is defined as the one for which the largest remaining intact piece being one half of the mass of the original. Note that Q^* is not specifically a material property, such as compressive strength, tensile strength, and so on, but a measure that depends on the impact conditions. Detailed discussion about strength is found in Holsapple (2008).

Generally, Q^* was shown to positively depend on static material strength for non-porous targets. A power-law relation determined between static strength and impact strength defined by energy density per volume of the larger body, Q^*_V, for various brittle materials including ice, tuff, and some rocks, is presented as

$$Q^*_V\,[erg/cm^3] = 0.12\{Y[erg/cm^3]\}^{0.84}, \quad (1)$$

where Y denotes compressive strength of the target material (Davis and Ryan 1990). This equation may be modified into the one of Q^* as follows,

$$Q^*[erg/g] = \frac{Q^*_V}{\rho}[erg/g] = 0.06\left(\frac{2g/cm^3}{\rho}\right)\{Y[dyn/cm^2]\}^{0.84},$$

$$Q^*[J/kg] = 6\times 10^{1.56}\left(\frac{2000kg/m^3}{\rho}\right)\left(\frac{Y}{100MPa}\right)^{0.84}. \quad (1')$$

where ρ denotes density.

In porous bodies, it is expected that pores play important but complicated roles in impact disruption. More porous material is weaker in static strength, while pores

suppress transmission efficiency of the impact energy throughout the body. Love et al. (1993) performed disruption and cratering experiments using porous sintered glass beads. Four different targets were prepared by changing the sintering temperature. The more porous targets were weaker in static condition. An empirical relationship was derived where targets with higher porosity have higher $Q*$ as

$$Q^*[erg/g] = 7.57\times10^6(1-\phi)^{-3.6}\{Y[kbar]\}^{0.45}, \qquad (2)$$

where ϕ denotes the porosity, that is, $1-\phi$ represents the filling factor. For convenience, we rewrite the above in a different unit as follows;

$$Q^*[J/kg] = 7.57\times10^2(1-\phi)^{-3.6}\left(\frac{Y}{100MPa}\right)^{0.45}. \quad (2')$$

In general, porosity ϕ and strength Y should be considered to be independent as will be shown for sintered glass beads targets later in Fig. 2. Therefore, if one performs a series of experiments where the two parameters are not directly correlated, then one can try to determine the dependence on each parameter separately. For example, in the experiments from which Love et al. derived Eq.2, two of the four different targets had similar porosity (37 and 39 %) but different compressive strength (44 and 7.9 MPa). Since the results of impact disruption experiment for these two targets were found to be consistent with a previously proposed empirical relationship between $Q*$ and Y (Horz et al. 1975), the same dependence was assumed for the results of the other two

targets, and Eq.2 was derived. However, the two parameters for the laboratory constructed sample usually have a correlation as will be described in Section 3 and it becomes complicated to sort out the separate effects of strength from porosity.

Arakawa et al. (2002) conducted experiments of pure ice and ice-silicate mixture targets with porosity up to 55 % and examined the effect of porosity not only upon the static strength but also on the initial peak pressure and the attenuation rate of the stress wave in target body. In their experiment, the impact strength of pure ice increased with increased target porosity, but interestingly, that of mixture target had an opposite tendency; that is the impact strength decreased with increase of porosity. The reason of the opposite tendency was attributed to a stronger dependence of the static strength upon porosity of the ice-silicate mixture targets (Arakawa and Tomizuka 2004). It is thus obvious that the outcome of impact disruption of porous targets is strongly dependent upon the structure and material composition of the targets.

In this review, we present a classification of porous targets in the literature (e.g., Martelli et al. 1994; Holsapple et al. 2002) and those of on-going laboratory impact experiments according to the internal structure, describe the physical properties of these materials, and summarize some results of impact strength. The porosity of the targets ranges from a few to over 80 %, while the compressive strength ranges from under 1

MPa to over hundreds of MPa.

2. Porous targets of different internal structures

Porous small bodies can be classified based on whether or not the body is an aggregate or a solid body with void spaces. Aggregate type porous structure includes a pile of rocks as the one extreme, where the individual component is strong enough in comparison with cohesive force between the components, and the binding force is primarily gravity. Such a structure is relevant for the impact-disrupted and re-accumulated body. If the component of the aggregate is fine enough, that is, in case of primordial dust aggregates and planetesimals, Van der Waals' force between the components results in finite strength (Greenberg et al.1995, Blum and Schra¨pler, 2004). This type corresponds to the "Coherent aggregates" or "Coherent rubble-pile" whose components are attached or cemented to one another with no explanation about the "glue," except that it is not gravity in comparison with "Gravitational aggregate" or "Gravitational rubble-pile" in a previous classification (see Richardson et al. 2002 for the definition). Weakly sintered aggregate is also classified into this group. Sintering process, that is a process of neck growth between particles under the melting temperature due to material movement toward the potential low of a curved surface

through such as surface diffusion etc., develops stronger bond between the component and will increase the strength of, for example, cometary bodies (Sirono 1999). Another type of porous bodies is the one with numerous cracks and flaws opened in a previously solid body by tensile stress caused by the rarefaction wave following the shock compression. This type is usually called as “Pre-shattered” or “Fractured” (e.g., Michel et al. 2003). Or the one with void spaces due to evaporation of volatile components, such as pumice.

Although self-gravity is the binding force of the “Gravitational aggregates” or “Gravitational rubble-pile”, it is difficult to simulate such bodies in the laboratory conditions. Therefore, previous impact disruption experiments of aggregate targets have been performed for coherent aggregates (or rubble-pile), except for the one of sand-bag, i.e., loosely bounded sand in a thin paper bag (Yanagisawa and Itoi 1994). One of the important parameters characterizing the aggregates is the strength of the component and the bond between the constituents. The ratio of the tensile strength of the object to mean tensile strength of the components is defined as relative tensile strength (RTS) and is used for a classification of the internal structure of small bodies (Richardson et al. 2002). Another important parameter is the size (or size distribution) of the pores and the constituents in comparison with minimum size scale of uniformity such as mineral grain

size, and with projectile size at collision. Porosity due to fractures, voids, and pores on the scale of tens of micrometer in meteorites is called as microporosity. On the other hand, large-scale voids and fractures on asteroids produced by the impact history of the asteroid are called macroporosity (Britt et al. 2002).

Porous targets with small RTS were prepared by pebbles and ice chips. Ryan et al. (1991) used targets of 42 % porosity in which strong constituent pebbles were weakly bounded together by very weak glue diluted with water, and studied the impact strength and the size distribution of the fragments. Ryan et al. (1999) and Giblin et al. (2004) conducted impact experiments using porous ice and snowball targets with porosity of 30-45 % (Ryan et al. 1999) and 39-54 % (Giblin et al. 2004) designed to simulate Kuiper Belt Objects (KBOs) in structure. Ice chips with different mass distributions were bounded together by partial melting and refreezing to form porous ice targets. Snowball targets were made of sub-mm size ice powders. These icy targets were too fragile to use conventional techniques for measuring mechanical strength. Coherent aggregate targets with increased bond strength were prepared by sintering of 50 □m-diameter glass beads (Love et al. 1993, Michikami et al. 2007, Setoh et al. 2007). The porosity of the weakly sintered targets is about 40 % and decreases with proceeding of the sintering process, i.e., growth of necks between the particles. Targets with

porosity of 60 and 80 % were prepared using hollow glass beads. Porous ice-silicate mixture targets made by pressure-sintering process were used to simulate icy small bodies such as icy satellites (Arakawa et al. 2002; Arakawa and Tomizuka 2004). The targets had measurable strength varying with porosity and fraction of the silicate content. Since the target's physical properties thus can be controlled by the fraction of the silicate content and sintering conditions and, in addition, the treatment is easier than those of icy materials, glass beads-rock powder mixture targets are used to study the impact process of porous targets with different physical properties (Hiraoka 2008). Coherent aggregate targets with hydrates, such as cement mortar and gypsum, have also been used for impact disruption experiments (Davis and Ryan 1990; Kawakami et al. 1991; Nakamura et al. 1992), because of multiple reasons. They are porous materials that are easy to be prepared, they may be good analogue of some hydrated meteorites and, therefore, asteroids, and the micro structure looks similar to those of some meteorites as shown in Figs. 1a and 1b. Figures 1a and 1b show scanning electron microscope (SEM) images of a gypsum target used in impact experiments (Fujii et al. 2008) and cut surface of Allende meteorite's matrix. Gypsum target consists of about 10 micron-sized particles and void space in similar size-scale of the grains that is microporosity. Porphyritic olivine basalt, consisting of millimeter-size olivine

phenocrysts in a fine-grained vesicular matrix was also used in order to simulate a stone meteorite (Durda and Flynn 1999).

Pre-shattered bodies are simulated by reconstruction of impact fragments into the shape of the original cement mortar targets using glue (Ryan et al. 1991). Fractured bodies were also simulated by the fragments or target itself from previous impact disruption experiments (Gault and Wedekind 1969; Nakamura et al. 1994). In the target preparation based on sintering process, highly porous structure was archived by using hollow glass beads (Love et al. 1993; Michikami et al. 2007). Pumice and perlite have void spaces due to evaporation of volatiles and have porosity as high as those of sintered hollow glass beads targets. Blocks of pumice were used in impact disruption experiments (Giacomuzzo et al. 2007), whereas perlite powders were used to form a very porous and fragile targets for impact cratering experiments (Housen and Holsapple 2003). Figure 1c shows internal structure of pumice with porosity of about 75 %. The internal microstructure is different form the ones shown in Figs. 1a and 1b.

3. Physical property of porous structure

3-1 Static strength and elastic constants

The static strength of porous material is usually lower than that of dense material, as indicated by an empirical formula known for ceramics (Ryshkewitch 1953), given by

$$Y = c_1 e^{-c_2(1-\phi)}, \quad (3)$$

where c_1 and c_2 are constants. Empirical expressions between the static compressive strength and porosity were given as a power-law of the filling factor as $Y = 9.8[MPa](1-\phi)^{3.4}$ and $Y = 9.5[MPa](1-\phi)^{6.4}$ for pure ice and ice-silicate mixture, respectively (Arakawa and Tomizuka 2004). Figure 2 shows the relation between porosity and uniaxial compressive strength of the target materials used in previous impact disruption experiments. Although the compressive strength is known to be dependent upon the size of the test specimen for solid materials, the values in Fig. 2 are the ones with no correction. Because when uniform-sized particles are randomly packed porosity becomes about 40 %, coherent aggregate targets with porosity about 40 % but with wide range of strength can be prepared by sintering process. Applying the same technique for particles with different size distribution or hollow particles, targets with wide range of porosity and strength will also be available.

Elastic constants give the measure of the stiffness of the structure. Figure 3 shows the P-wave and S-wave velocities of gypsum (Kawakami et al. 1991; Fujii et al. 2008) and pumice. The pumice data and Fujii et al.'s gypsum data are the calculated ones from

Young's modulus and shear modulus determined by measurements of natural resonance frequencies of bending and torsional vibration of plates of the material. The data of Fujii et al.'s gypsum show that the wave velocities increase with decrease of the porosity. In Fig. 3, the values of targets used in impact disruption experiments and those of ordinary chondrite meteorites are shown (Yomogida and Matsui 1983; Takagi et al. 1984; Nakamura and Michel 2008). The data of gypsum and pumice are in the range of the values of ordinary chondrite meteorites. The ratio of the P-wave and S-wave velocities, V_p and V_s respectively, gives the Poisson's ratio of the material ($=\frac{V_p^{\,2}-2V_s^{\,2}}{2(V_p^{\,2}-V_s^{\,2})}$). The clear relationship between P-wave and S-wave velocities shown here indicates that all the samples have similar Poisson's ratio.

3-2 Crush curve

Impact disruption of porous bodies with flaws and voids larger than the resolution of simulation can be directly treated with pre-exiting numerical code for solid materials, however porous bodies with porosity less than the numerical resolution limit needs a model accounting for compaction (Wunnemann et al. 2006; Jutzi et al. 2008). Relation between applied load and distension which is given by

$$\alpha = \frac{1}{1-\phi}, \quad (4)$$

is basic laboratory data for a porous-compaction model. The relation for various porous medium was obtained by the compression testing machine installed at Kobe University. The sample was put in a hollow cylinder made by stainless steel and whose inner diameter was 9.95 mm and was compressed by a stainless steel cylinder head tightly fit to the hollow cylinder. The loading rate was 0.001 mm/s and 0.1 mm/s. Figure 4 shows examples of distension-load (per unit area) relation, crush curve, of gypsum, pumice, sintered and non-sintered glass beads, and spherical silica particles of the similar size of the gypsum grains, 10 μm. The particle diameter of the sintered and non-sintered glass beads is about 50 μm. The measurement of silica particles was performed using a hollow cylinder and a head of 5 mm diameter, respectively.

The gypsum, pumice, and sintered glass-beads samples were compressed quasi-elastically until they were destructed at about the load level corresponding to the uniaxial compressive strength of the material. After the destruction, the samples seemed to be compressed plastically, where probably destruction of weakest parts of the samples and rearrangement of the constituents occurred in microscopic scale. On the other hand, granular materials, i.e., glass bead and silica particles show no clear elastic-plastic transition. The curve of the sintered glass beads approaches toward that of

the glass beads after the first major destruction, with wavy structure in the curve due to further destruction of the structure. The value of the compressive strength of the glass beads provided by manufacturer is about 800 MPa, which is much larger than the maximum pressure archived in these measurements. In fact, disruption of individual glass bead was not obvious in the fragments after the compression test. Thus, in case of sintered glass beads, the porosity was probably decreased by relocation of the beads that could move freely because the necks can be broken by the compression within the applied load of the present static test. Although the initial packing density of the glass beads was already close to the maximum packing density of 63.7 % experimentally determined for dense random packing (Scott 1960), the decrease of the porosity was available probably because the glass beads were not mono-disperse but had some range in its diameter. Pumice curve has similar wavy structure with various amplitudes probably due to the destruction of pores of various sizes shown in the SEM image of Fig.1. On the other hand, gypsum curve shows oscillation of several MPa in amplitude, probably due to the destruction of bonds between individual grains. Another explanation of the wavy structure of the curves may be just friction on the walls of the cylinder, however, the smooth structure of the curves of glass beads and silica particles supports the former explanation.

The curves of the 50 μm glass beads and the plastic region of the sintered glass beads and the pumice are not different between the two loading rates. However, preliminary measurement results of the curves of the gypsum at different loading rate were slightly different, despite only small difference in the loading rate in comparison with the difference between dynamic and static tests where the dynamic stiffening was observed for powders (Vogler et al. 2007). Further investigation of the strain rate dependence in crush curve is required.

4 Impact strength

Figure 5 summarizes the data of impact strength Q^* of porous materials in comparison with the results of brittle solid materials such as basalt and the empirical relation given by Eq.1' for materials with density ρ of 2 g cm^{-3}. Although the impact strength of solid material increases almost monotonically with the static compressive strength, the impact strength of porous materials is scattered, although all the data points are above the line for the solid materials meaning that porous materials are stronger against impact disruption than solid materials as expected. Previous laboratory studies indicated that impact strength at lower velocity collision is lower than the one at higher velocity collision (e.g., Ryan et al 1991; Kawakami et al. 1991; Setoh et al. 2007). The

two gypsum points are derived from the high (2850 – 4170 m/s) and low (100 - 758 m/s) velocity impact experiments of Kawakami et al. (1991). Dashed line shows an empirical relation of Eq.1' for sintered glass beads target based on disruption experiments performed at high velocity (4851-5483 m/s) (Love et al. 1993), whereas the other two data points are from low velocity impact experiments (<100m/s) (Setoh et al. 2007). Impact velocity dependence for the impact strength was also predicted by previous scaling theories (e.g. Housen and Holsapple 1990; Mizutani et al. 1990). The velocity dependence is represented by a simple power-law function of the impact velocity by the scaling theory of Housen and Holsapple (1990) as $Q^* \propto U^{2-3\mu}$, where U is impact velocity and μ is a parameter that is about 0.4 for porous materials such as dry sand. We can see this scaling theory thus predict the about an order of magnitude difference in Q* for tests with impact velocities of an order of magnitude difference.

Setoh et al. (2007) showed that impact strength of sintered glass beads targets with a fixed porosity of about 40 % at low impact velocity condition increases with the static strength with a power of about 1. This fact can be interpreted as that the propagation efficiency of the stress wave in the target is almost insensitive to the size of the necks between the sintered glass particles for the targets with a fixed porosity. Study of the attenuation rate of the stress wave through the target will give further understanding.

Yanagisawa and Itoi (1994) conducted impact experiments at high velocity (3.7 - 7.3 km/s) onto porous targets, studied the antipodal ejection velocity with relation to the distance from a point called “equivalent center”, the center of the propagation of the stress wave, and then compared it with the value expected when the attenuation of the stress wave occurs with a power m of -3 with the distance. It was shown that the attenuation is more significant for sand than mortar and porous alumina, although the porosity of the sand target is between those of mortar and porous alumina. The fact shows that the attenuation rate, and then the impact strength, is dependent upon not only porosity but also the internal structure that may be represented by RTS. Arakawa et al. (2002) proposed a relation between the power index of the attenuation rate and porosity as

$$m = m_0(1-\phi)^{-k} \quad , (5)$$

where they chose m_0=-2 and k=0.5 for the porous ice and porous ice-silicate mixture. Further quantitative investigation is required about the dependence of the attenuation rate of the stress wave upon porosity and the relation with the crush curve.

5 Conclusion

Our understanding of impact process of porous bodies has been grown thanks to

impact experiments of targets with wide range of porosity and strength. However, much to be investigated before quantitative understanding is established. There are several potentially important parameters that control the outcome of the impact disruption of porous bodies, such as porosity, strength, RTS, and impact velocity. Although flaw statistics of the target body is widely accepted as one of key parameters that determine the outcome of the impact disruption of solid targets (Housen and Holsapple 1999, Nakamura et al. 2007), little is known about the role of crack growth in the disruption of porous bodies. Similarly, the effect of compaction on the strength of the target is to be understood. Compaction may increase compressive strength; however, it often breaks bonds between constituent, increases damage in the material (Jutzi et al. 2008) and decreases RTS. On the other hand, spin of the body was shown to have large effect on impact disruption of porous targets (Housen 2004). Impact experiments with porous targets with detailed characterization of material properties will be useful to establish a database that can serve as a reference for numerical modeling and theoretical scaling considerations.

Acknowledgements

We thank Y. Fujii and K. Iinuma for providing SEM images of gypsum and Allende

matrix. We also thank K. Sangen for preparation of the stainless-steel cylinders used in the crush curve measurement. Acknowledgements also go to P. Michel, M. Arakawa, and M. Setoh for fruitful discussions. This research was supported by grants-in-aid for science research from the Japanese Society for the Promotion of Science (No. 19015007) and Kobe University through "The 21st Century COE Centers of Excellence Program of the Origin and Evolution of Planetary Systems", of the Ministry of Education, Culture, Sports, Science and Technology (MEXT), Japan.

References

Arakawa, M., Leliwa-Kopystynski, J., and Maeno, N., 2002. Impact experiments on porous icy-silicate cylindrical blocks and the implication for disruption and accumulation of small icy bodies, Icarus 158, 516-331.

Arakawa, M. and Tomizuka, D., 2004. Ice-silicate fractionation among icy bodies due to the difference of impact strength between ice and ice-silicate mixture, Icarus 170, 193-201.

Britt, D. T., Yeomans, D., Housen, K., et al., 2002. Asteroid density, porosity, and structure, in: W. F. Bottke, Jr. et al. (Eds), Asteroids III, Univ. of Arizona Press, Tucson, pp. 485-500.

Blum, J., and Schra¨pler, R., 2004. Structure and mechanical properties of high-porosity macroscopic agglomerates formed by random ballistic deposition, Phys. Rev. Letters, 93, id.115503.

Davis, D. R., and Ryan, E. V., 1990. On collisional disruption - Experimental results and scaling laws, Icarus 83, 156-182.

Durda, D. D. and Flynn, G. J., 1999, Experimental study of the impact disruption of porous, imhomogeneous targets, Icarus 142, 46-55.

Fujii, Y., Nakamura, A.M., and Hiraoka, K., 2008. Laboratory experiments of

compaction and fragmentation of porous bodies at low velocity collisions, 39th Lunar and Planetary Science Conference, LPI Contribution No.1391., p. 1934.

Fujiwara, A., Kawaguchi, J., Yoemans, D. K., et al., 2006. The rubble-pile asteroid Itokawa as observed by Hayabusa, Science, 312, 1330-1334.

Gault, D.E. and Wedekind, J.A. 1969. The destruction of tektites by meteoroid impact, J. Geophys. Res., 74, 6780-6794.

Giacomuzzo, C., Ferri, F., Bettella, A., et al., 2007. Hypervelocity experiments of impact cratering and catastrophic disuruption of targets representative of minor bodies of the Solar System, Adv. Space Res., 40, 244-251.

Giblin, I., Davis, D. R., and Ryan, E. V., 2004. On the collisional disruption of porous icy targets simulating Kuiper belt objects, Icarus, 171, 487-505.

Greenberg, J.M., Mizutani , H., and Yamamoto, T., 1995. A new derivation of the tensile strength of cometary nuclei: Application to comet Shoemaker-Levy 9, Astronomy and Astrophysics, 295, L35-L38.

Hiraoka, K., 2008. Experimental study of the impact cratering process in the strength regime, Ph.D. thesis, Kobe University.

Holsapple, K., 2008. On the “strength” of the small bodies of the solar system: A review of strength theories and their implementation for analyses of impact disruptions.

Planet. Space Sci. doi:10.1016/j.pss.2008.05.015 .

Holsapple, K., Giblin, I., Housen, K et al., 2002. Asteroid impacts: laboratory experiments and scaling laws, in: W. F. Bottke, Jr. et al. (Eds.), Asteroids III, Univ. of Arizona Press, Tucson, pp. 443-462.

Horz, F., Schneider, E., Gault, D.E., et al., 1975. Catastrophic rupture of lunar rocks: A Monte Carlo simulation, The Moon 13, 235-258.

Housen, K., 2004. Collision fragmentation of rotating bodies, 35th Lunar and Planetary Science Conference, abstract no.1826.

Housen, K. R. and Holsapple, K. A., 1990. On the fragmentation of asteroids and planetary satellites, Icarus 84, 226-253.

Housen, K. R. and Holsapple, K. A., 1999. Scale effects in strength-dominated collisions of rocky asteroids, Icarus 142, 21-33.

Housen, K.R. and Holsapple, A., 2003. Impact cratering on porous asteroids, Icarus 163, 102-119.

Jutzi, M., Benz, W., and Michel, P., Implementing micro-scale porosity in a 3D SPH Hydrocode, Icarus, submitted.

Kawakami, S., Kanaori, Y., Fujiwara, A. et al., 1991. An experimental study of impact fracturing of small planetary bodies in the solar system with an application to

PHOBOS, Astron, Astrophys. 241, 233-242.

Love, S. G., Hörz, F., and Brownlee, D. E. 1993. Target porosity effects in impact cratering and collisional disruption, Icarus, 105, 216-224.

Martelli, G., Ryan, E.V., Nakamura, A.M., and Giblin, I. 1994. Catastrophic disruption experiments: recent results, Planet. Space Sci. 42, 1013-1026.

Michel, P., Benz, W. and Richardson, D.C. 2003. Disruption of fragmented parent bodies as the origin of asteroid families, Nature 421, 608-611.

Michikami, T., Moriguchi, K., Hasegawa, S., et al. 2007. Ejecta velocity distribution for impact cratering experiments on porous and low strength targets, Planet. Space Sci, 55, 70-88.

Mizutani, H., Takagi, Y., and Kawakami, S.-I., 1990. New scaling laws on impact fragmentation, Icarus, 87, 307-326.

Nakamura, A., Suguiyama, K., and Fujiwara, A. 1992. Velocity and spin fragments from impact disruptions. I - an experimental approach to a general law between mass and velocity, Icarus 100, 127-135.

Nakamura, A.M., Fujiwara, A., Kadono, T., and Shirono, S. 1994. Fragmentation of intact and pre-impacted basalt targets, In Seventy-Five Years of Hirayama Asteroid Families, ASP Conference Series, 63, 237-242.

Nakamura, A.M., Michel, P. and Setoh, M. 2007. Weibull Parameters of Yakuno Basalt Targets Used in Documented High-Velocity Impact Experiments, J. Geophys. Res. (Planets) 112, 10.1029/2006JE002757.

Nakamura, A. M., Michikami, T., Hirata, N., Fujiwara, A., Nakamura, R., Ishiguro, M., Miyamoto, H., Demura, H., Hiraoka, K., Honda, T., Honda, C., Saito, J., Hashimoto, T., Kubota, T. 2008. Impact Process of Boulders on the Surface of Asteroid 25143 Itokawa -Fragments from Collisional Disruption, Earth Planet. Space, 60, 7-12.

Nakamura, A. M., and Michel, P., 2008. Asteroids and their collisional disruption, in Small bodies in planetary systems (Eds. Mann, I, et al.), Lecture series in physics, Springers Lecture Notes in Physics Series, accepted.

Richardson, D.C., Leinhardt, Z.M., Melosh, H.J., et al. 2002. Gravitational aggregates: Evidence and evolution, in: W. F. Bottke, Jr. et al. (Eds.), Asteroids III, Univ. of Arizona Press, Tucson, pp. 501-515.

Ryan, E. V., Hartmann, W., and Davis, D., Impact experiments 3: catastrophic fragmentation of aggregate targets and relation to asteroids. Icarus 94, 283-298, 1991.

Ryan, E, V., Davis, D, R., Giblin, I., A laboratory impact study of simulated Edgeworth-Kuiper Belt Objects, Icarus, 142, 56-62, 1999.

Ryshkewitch, E., Compression strength of porous sintered alumina and zirconia, J. Am. Ceram. Soc., 36, 65-68, 1953.

Scott, D. G., 1960. Packing of Spheres: Packing of Equal Spheres, Nature 188, 908-909.

Setoh, M., Nakamura, A, M., Hiraoka, K., et al. Collisional disruption of weakly sintered porous targets at low impact velocities, Earth Planet. and Space, 59 319-324, 2007.

Sirono, S. Effects by sintering on the energy dissipation efficiency in collisions of grain aggregates, Astronomy and Astrophysics, 347, 720-723, 1999.

Takagi, Y., Mizutani, H., and Kawakami, S. –I., 1984. Impact fragmentation experiments of basalts and pyrophyllites, Icarus 59, 462-477.

Vogler, T. J., Lee, M. Y., and Grady, D. E., 2007. Static and dynamic compaction of ceramic powders, Int. J. Sol. St., 44, 636-658.

Wunnemann, K., Collins, G.S., and Melosh, H.J., 2006. A strain-based porosity model for use in hydrocode simulations of impacts and implications for transient crater growth in porous targets, Icarus 180, 514-527.

Yanagisawa, M., and Itoi, T., 1994. Impact fragmentation experiments of porous and weak targets, Proc. Seventy-five (75) years of Hirayama asteroid families: The role of collisions in the solar system history, Astronomical Society of the Pacific

Conference Series (Eds. Kozai, Y., Binzel, R.P., and Hirayama, T.), 63, 243-250.

Yomogida, K., and Matsui, T., 1983. Physical properties of ordinary chondrites, J. Geophys. Res., 88, 9513-9533.

Figure caption

Figures 1 Scanning electron microscope images of materials with micro posority. (a) Surface of a gypsum target used for low velocity impact experiments (Fujii et al. 2008), (b) Cut surface of Allende meteorite's matrix, and (c) pumice of Ito ignimbrite from Aira caldera, Japan.

Figure 2 Porosity and compressive strength of the materials used in impact disruption experiments: sintered glass beads with and without hollow glass beads (Love et al. 1993; Setoh et al. 2007), gypsum (Kawakami et al. 1991; Fujii et al. 2008), pebble aggregate (Ryan et al. 1991), mortar and preshattered mortar (Davis and Ryan 1990; Ryan et al. 1991; Yanagisawa and Itoi 1994), porous alumina (Yanagisawa and Itoi 1994), and pure ice and ice-silicate mixture (Arakawa and Tomizuka 2004), and pumice.

Figure 3 Compressive and shear wave velocities of the materials used in impact disruption experiments: basalt and pyrophyllite (Takagi et al. 1984), gypsum (Kawakami et al. 1991; Fujii et al. 2008), and pumice. The data of ordinary chondrite meteorites are also shown (Yomogida and Matsui 1983).

Figure 4 Crush curve of gypsum, pumice, sintered and non-sintered glass beads, and spherical silica particles of 10 μm in diameter. The compressive strength of the gypsum, sintered glass beads, and pumice were measured using two other specimens and found to be 17.1+/-5.1, 9.5+/-3.6, and 5.1+/-0.1 MPa, respectively. (a) The curves for full range of measurement. (b) An expanded view of the same data in (a).

Figure 5 Impact strength Q* of porous materials in comparison with the results of brittle solid materials such as basalt and the empirical relation given by Eq.1' for materials with density ρ of 2 g cm^{-3}. The upper gypsum point is derived from the high (2850 – 4170 m/s) velocity impact disruptions and the lower point is from the low (100 - 758 m/s) velocity impacts (Kawakami et al. 1991). The filled circles show the data from previous low-velocity laboratory experiments of sintered glass beads targets with directly measured compressive strength (Setoh et al. 2007). Data points of basalt are from the compilation of Takagi et al. (1984). Number in parenthesis indicates porosity.

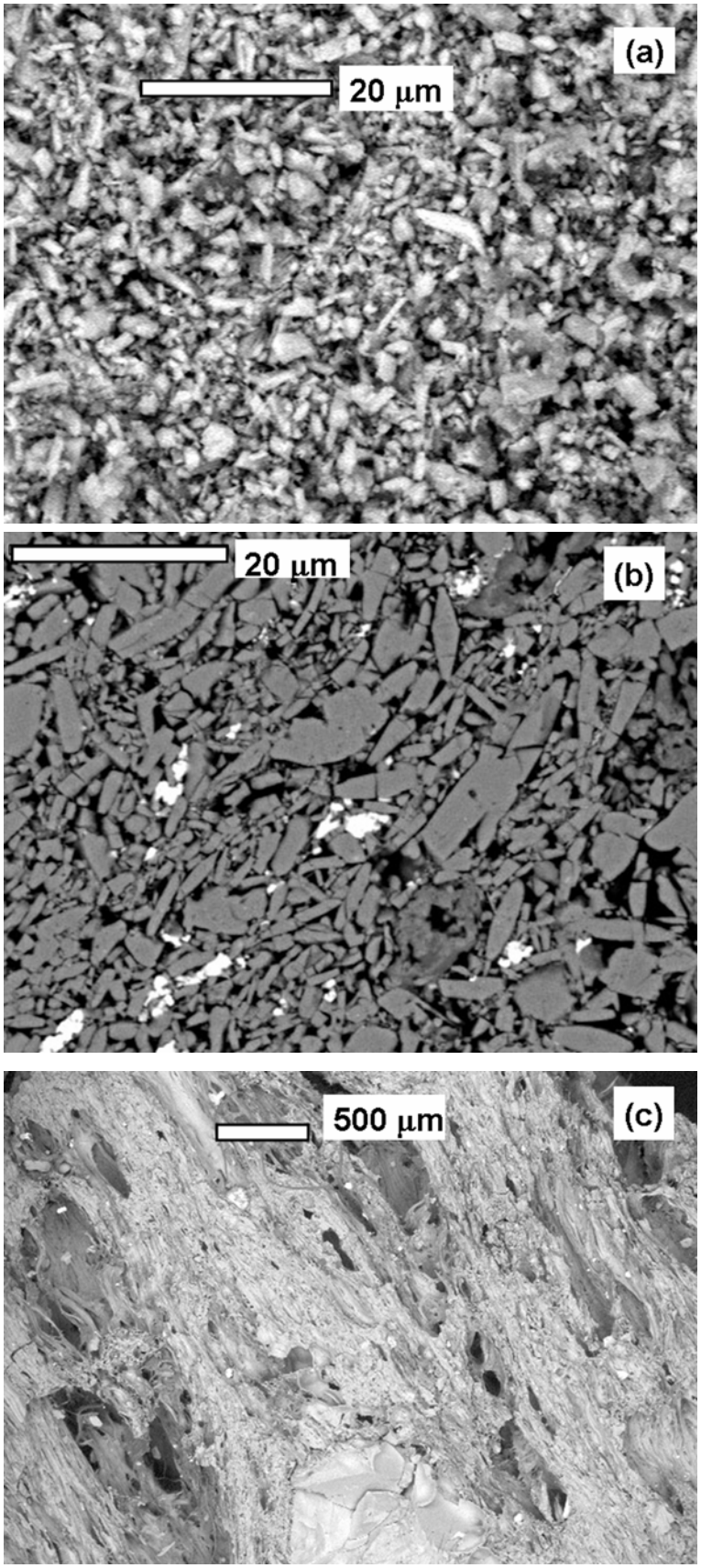

Fig.1

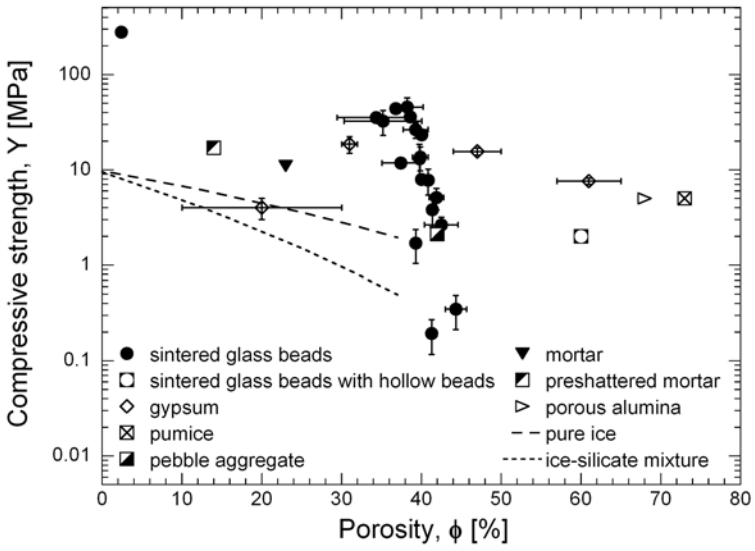
Compressive strength, Y [MPa]
100
10
1
0.1
0.01
0
10
20
30
40
50
60
70
80
Porosity, ϕ [%]
sintered glass beads
sintered glass beads with hollow beads
gypsum
pumice
pebble aggregate
mortar
preshattered mortar
porous alumina
pure ice
ice-silicate mixture

Fig.2

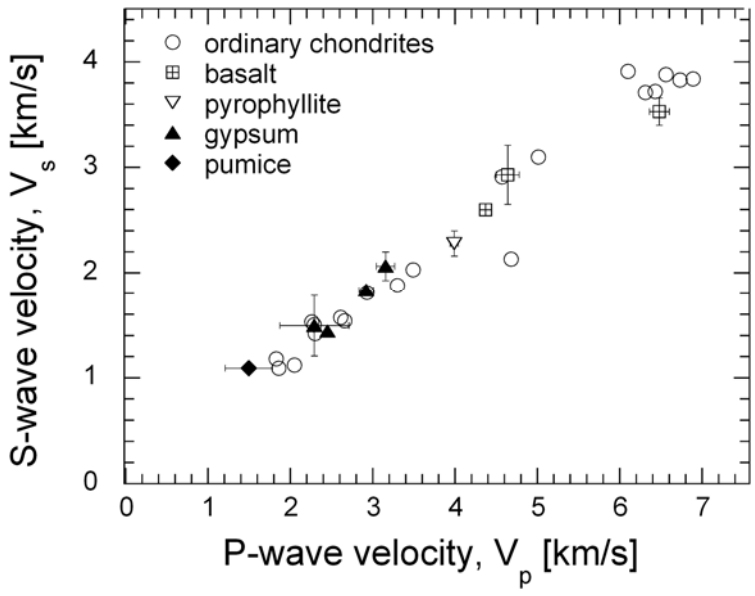
S-wave velocity, V_s [km/s]
0
1
2
3
4
0
1
2
3
4
5
6
7
P-wave velocity, V_p [km/s]
ordinary chondrites
basalt
pyrophyllite
gypsum
pumice

Fig.3

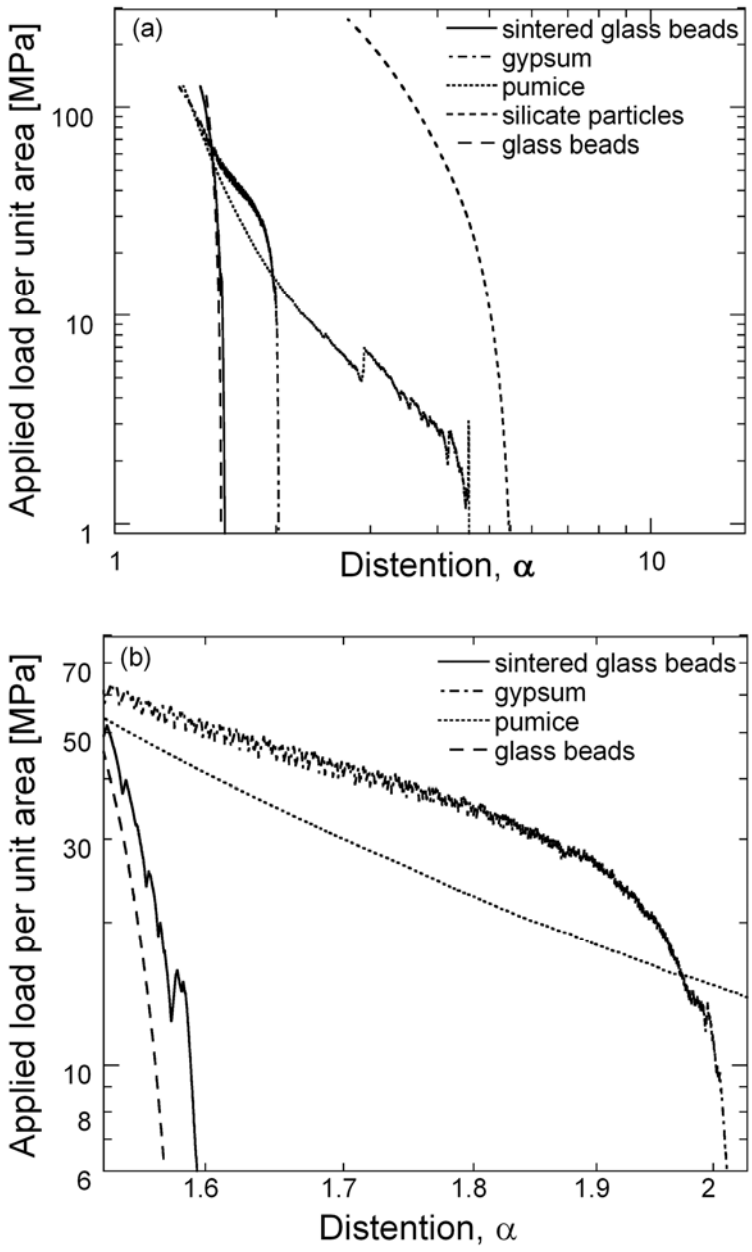
(a)
sintered glass beads
gypsum
pumice
silicate particles
glass beads
Applied load per unit area [MPa]
100
10
1
1
10
Distention, α
(b)
sintered glass beads
gypsum
pumice
glass beads
Applied load per unit area [MPa]
70
50
30
10
8
6
1.6
1.7
1.8
1.9
2
Distention, α

Fig.4

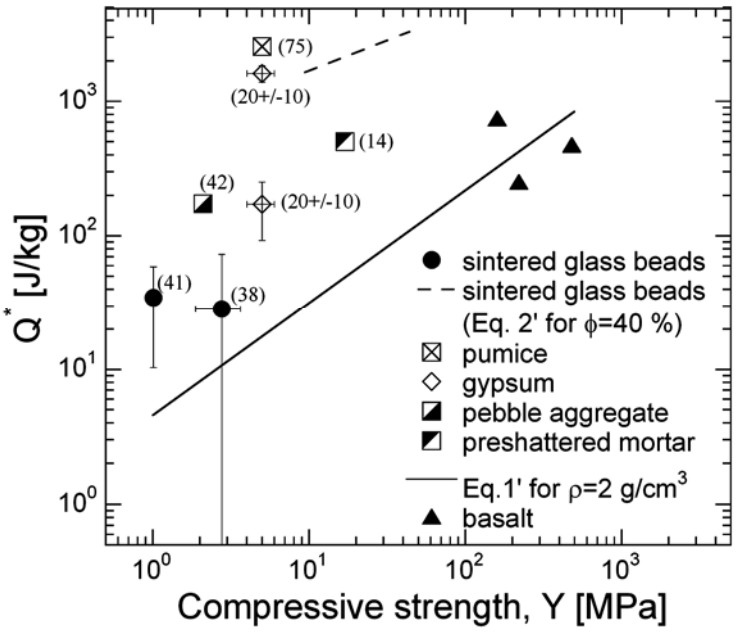
(75)
(20+/-10)
(14)
(42)
(20+/-10)
(41)
(38)
sintered glass beads
sintered glass beads
(Eq. 2' for ϕ=40 %)
pumice
gypsum
pebble aggregate
preshattered mortar
Eq.1' for ρ=2 g/cm3
basalt
Q* [J/kg]
Compressive strength, Y [MPa]

Fig. 5